Decoding concealed information using multimodal neurophysiological signals

Sruthi Sundharram[1], Santosh Kottasamu[2], Krishna Ika[2], and Ramana Vinjamuri[1,*]

[1]Vinjamuri Lab, Department of Computer Science and Electrical Engineering, University of Maryland Baltimore County, Baltimore, MD 21250, USA
[2]Brainwave Science Inc., USA
[*]Email: rvinjam1@umbc.edu

ABSTRACT

Detecting concealed information is a critical challenge in forensic investigations, security screening, and cognitive neuroscience. Conventional approaches using the Concealed Information Test primarily rely on binary classification, distinguishing between recognized (concealed) and unrecognized (neutral) stimuli. This limits interpretability and fails to reveal the nature of the concealed knowledge. In this study, we present a novel multimodal framework that moves beyond binary detection by decoding the category of concealed information into object, person, or place based on neurophysiological signals recorded during a concealed information test. High density electroencephalography and physiological signals, including skin temperature, galvanic skin response, and photoplethysmogram, were simultaneously recorded from ten subjects as they viewed visual stimuli representing these three categories. Temporal and spectral features were extracted from both modalities, followed by machine learning based multimodal fusion for classification. The proposed framework achieved an overall accuracy of 94.2%, significantly outperforming unimodal EEG (73%) and physiological (54.2%) baselines. Further analysis showed that similar decoding performance can be achieved using as few as eight strategically selected EEG electrodes, supporting the feasibility of lightweight, wearable implementations. The most informative electrodes were located over prefrontal and frontocentral regions, aligning with cognitive processes related to attention, recognition, and deception. These findings demonstrate that neurophysiological signals enables not only the detection of concealed knowledge but also the identification of the type of hidden information. The integration of EEG and physiological signals enhances both sensitivity and interpretability by capturing complementary aspects of cognitive and affective processing during recognition. By enhancing the CIT paradigm from binary recognition toward semantic decoding, this study advances the development of interpretable deception detection systems and bridges laboratory neuroscience with real world forensic applications.

Introduction

Deceptive behavior is a core feature of human interaction, and the ability to determine whether individuals possess concealed knowledge remains a central challenge in forensic science, intelligence operations, security screening, and applied cognitive neuroscience. In many investigative contexts, a person may recognize critical details about an event yet deliberately suppress any outward sign of that recognition. For more than a century, researchers and practitioners have turned to physiological measurement based on the premise that mental processes leave measurable traces in the body. Because recognition, emotion, and intentional concealment depend on neural activity and interact closely with autonomic systems, changes in physiology often accompany attempts to hide information. Early methods relied largely on observation, but advances in measurement technology made it possible to record subtle physiological signals with increasing precision, shaping the modern field of psychophysiological deception detection[1–4]. Reliable techniques for identifying hidden knowledge can sharpen investigative focus and provide insight into internal cognitive states that are not evident from behavior alone.

One of the most widely used paradigms for detecting concealed knowledge is the Concealed Information Test (CIT), a psychophysiological method derived from Lykken's Guilty Knowledge Test, which originally relied on galvanic skin response (GSR) measurements[5]. The CIT is closely related to the oddball paradigm, a well-established design in cognitive neuroscience in which infrequent "deviant" stimuli are embedded among frequent "standard" stimuli. In typical oddball tasks, rare targets evoke a larger P300 component of the event-related potential (ERP) compared to standard stimuli[6]. In the CIT, the frequent "irrelevant" stimuli correspond to standards, whereas the rare "probe" item, information known only to someone with knowledge acts as the deviant. Numerous P300 based CIT studies have shown that knowledgeable individuals produce a significantly larger P300 to probe items than to irrelevant items, mirroring the classic oddball effect[7–9]. Framing the CIT within this paradigm highlights the cognitive and neurophysiological mechanisms through which meaningful stimuli elicit differential cortical responses, thereby revealing concealed knowledge[10–12].

Traditionally, CIT based systems have focused on binary classification, distinguishing between "known" (concealed) and "unknown" (neutral) stimuli[13,14]. While effective, this approach provides limited interpretability, offering no insight into the nature of the concealed content. Early research primarily relied on electrodermal activity or GSR, particularly skin conductance responses[5,15–17], which reflect sympathetic arousal and increase in response to probe items. Electroencephalogram (EEG) especially the P300 component, provides higher temporal specificity and sensitivity to attentional relevance[18–20]. However, EEG based CITs are susceptible to noise, individual variability, and often require averaging across trials. Although both modalities are effective individually, relatively few studies have integrated EEG and GSR[21–23], and multiclass classification of concealed content remains largely unexplored.

In addition to EEG and GSR, studies have incorporated photoplethysmography (PPG) and skin temperature lie detection and concealed information paradigms. PPG provides a non invasive measure of cardiovascular activity, including heart rate and heart rate variability(HRV), which have been shown to reliably differentiate deceptive from truthful responses during the CIT[24–26]. Skin temperature, measured via thermal imaging, captures vasomotor changes mediated by the sympathetic nervous system, reflecting arousal and orienting responses elicited by crime relevant stimuli[27–29]. Both modalities offer complementary temporal profiles usefult to detect hidden mental states[30,31]; PPG is sensitive to rapid, phasic cardiovascular changes associated with orienting and recognition, while skin temperature captures slower, sustained autonomic shifts in response to salient stimuli.

Multimodal integration leverages the complementary strengths of central(EEG) and autonomic (GSR) nervous system measures. EEG captures rapid neural dynamics reflecting stimulus recognition and attentional processes, whereas GSR indexes sympathetic arousal associated with emotional and cognitive engagement. By integrating PPG, skin temperature, GSR along with EEG , our multimodal approach can capture a richer spectrum of autonomic cortical interactions. By combining these signals, it is possible to enhance sensitivity to concealed information, reduce susceptibility to noise or individual variability, and potentially achieve accurate single trial classification. This approach aligns with emerging trends in affective and cognitive neuroscience, where multimodal data fusion improves prediction of internal cognitive states[32,33].

Evidence from cognitive neuroscience and machine learning further supports the feasibility of multiclass decoding. Different categories of visual stimuli, such as faces, objects, and places, elicit separable cortical activation patterns[34,35], and multimodal approaches have demonstrated improved performance in affective computing and cognitive workload estimation[32,33]. Together, these findings suggest that a multimodal CIT could go beyond binary detection to decode not only whether information is concealed, but also what type of information is concealed.

While previous studies have shown the potential of psychophysiological measures for detecting deception, there is still a need for integrated frameworks that link physiological responses to the underlying cognitive processes of recognition. A multimodal decoding approach can help bridge this gap by combining neurophysiological signals to capture both arousal and attentional mechanisms involved in concealed knowledge. Beyond improving classification accuracy, such integration can provide better interpretability of how different neurophysiological systems interact when a person recognizes hidden information. Advancing in this direction can move the CIT from a purely detection based method toward a deeper understanding of the cognitive dynamics of concealment.

In this study, we introduce a novel multimodal framework for decoding the category of concealed information during a CIT. Subjects were presented with visual stimuli representing persons, objects, or locations while high density EEG and physiological data were recorded. By extracting temporal and spectral features and applying a machine learning based fusion strategy, we trained classifiers capable of predicting the category of concealed knowledge. Our results demonstrate that the multimodal approach significantly outperforms unimodal EEG and physiological baselines, enabling richer and more interpretable deception detection. These findings provide a foundation for future research in cognitive state decoding, neural semantics, and advanced lie detection systems.

The key contributions of this study are as follows:

1. Development of a multimodal CIT framework integrating EEG, GSR, plethysmography, and skin temperature to capture complementary neurophysiological and autonomic signals associated with concealed knowledge.
2. Introduction of multiclass concealed information decoding, moving beyond traditional binary detection to classify the type of concealed information (object, person or place).
3. Robust classification is made possible by applying machine learning-based multimodal fusion that combines temporal, spectral, and autonomic information.
4. Demonstration that comparable decoding performance can be achieved using a reduced set of strategically selected EEG electrodes, supporting the feasibility of lightweight and wearable implementations.
5. Empirical validation showing that the multimodal approach significantly outperforms unimodal EEG or physiological baselines, establishing a foundation for more accurate and generalizable deception detection systems with potential applications in forensic and security.

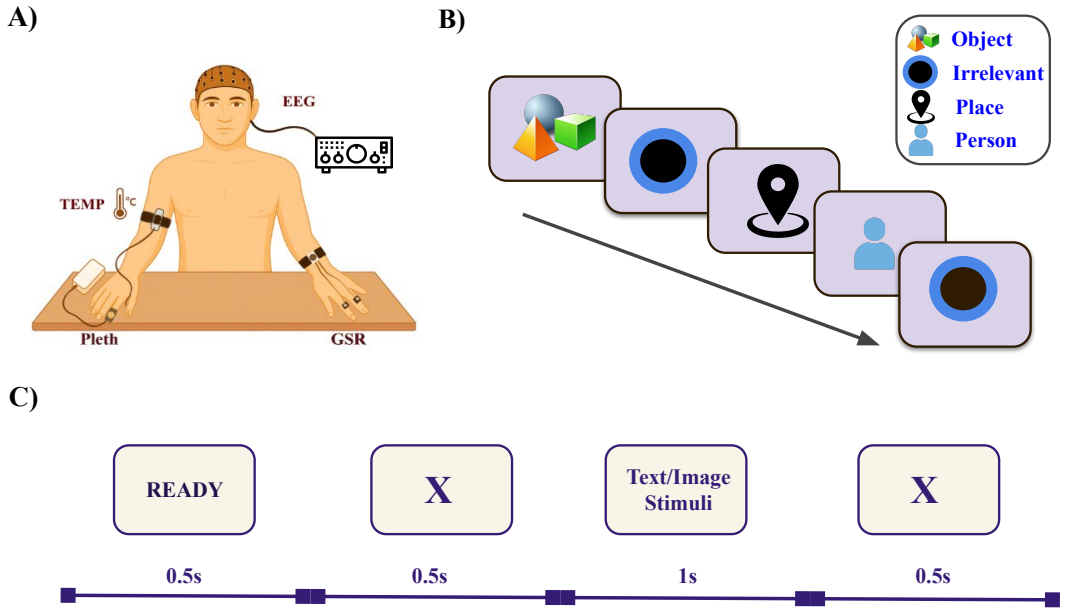

Figure 1. Experimental setup and task paradigm. (**A**) Schematic of the multimodal neurophysiological recording system, including EEG, skin temperature (Temp), plethysmogram (Pleth), and GSR sensors acquired during the CIT. (**B**) Visual oddball paradigm illustrating the four stimulus categories: object, person, place, and irrelevant presented to participants during the CIT. (**C**) Configuration of the stimulus presentation environment used for data acquisition.

Methods

Experimental design protocol and Data collection

Subjects

Ten healthy subjects (7 males, 3 females; age range: 22–26 years) participated in the experiment. Subjects were informed about the experiment and consent was obtained from all individuals. The experiment conduction and data collection were under an approved protocol by the Internal Review Board (IRB) of the University of Maryland Baltimore County.

Experimental Paradigm

The experiment consisted of two phases: (1) a text-based, and (2) an image-based. Each phase included five trials of approximately 300 seconds duration. Each trial contained 10 unique stimuli (targets, probes, and irrelevants), repeated five times in randomized order, totaling 50 stimuli per trial. Probe stimuli were highly personal in nature, such as the name of the participant's home country, a significant person, or a personally meaningful object. Target stimuli were known in advance and required a behavioral response; examples included the name of the university or current place of residence (place). Irrelevant items were neutral and unrelated to the participant. Figure 1B depicts the visual oddball paradigm presented to subjects during the CIT across the different stimulus categories: object, person, place, and irrelevant. Each stimulus was preceded and followed by a fixation cross ("x") displayed for 0.5 s. The stimulus itself (text or image) was presented for 1s as shown in Figure 1C. Subjects responded using an Microsoft Xbox wireless controller: **L1** was pressed for targets, and **R1** for all other stimuli (probes and irrelevants). Responses were instructed to be "long presses" to reduce variability in motor reaction times.

High Density EEG Recording

EEG was recorded using a 64 electrode g.tec EEG cap and g.HIamp amplifier system (g.HIamp, g.tec medical engineering GmbH, Graz, Austria). The left mastoid (*A1*) served as the reference and *AFz* as the ground. All signals were recorded in bipolar mode at a sampling rate of 600 Hz. Online filtering included a 0.01–30 Hz bandpass and a 58–62 Hz notch filter.

iCognative® Technology

Brainwave Science, Inc. has developed the proprietary iCognative® system, a commercial EEG based platform and a wearable device designed for concealed information detection using the P300 event related potential. The technology integrates electrophysiological and biometric measurements within an autonomous software system aimed at applications in national security, intelligence, defense, and law enforcement investigations. iCognative® leverages real time P300 based brainwave analysis to determine whether an individual recognizes specific stimuli, thereby facilitating the identification of concealed knowledge. In the present study, we adopted the same electrode configuration used in the iCognative® headset (*Fp1, Fp2, Cz1, Cz2, Cz3, Pz1, Pz2, Pz3*) to benchmark and compare our results against a wearable, low density EEG configuration. This comparison was conducted solely to assess the feasibility of achieving comparable classification performance with a limited number of strategically positioned electrodes benchmarked against research and industry standards.

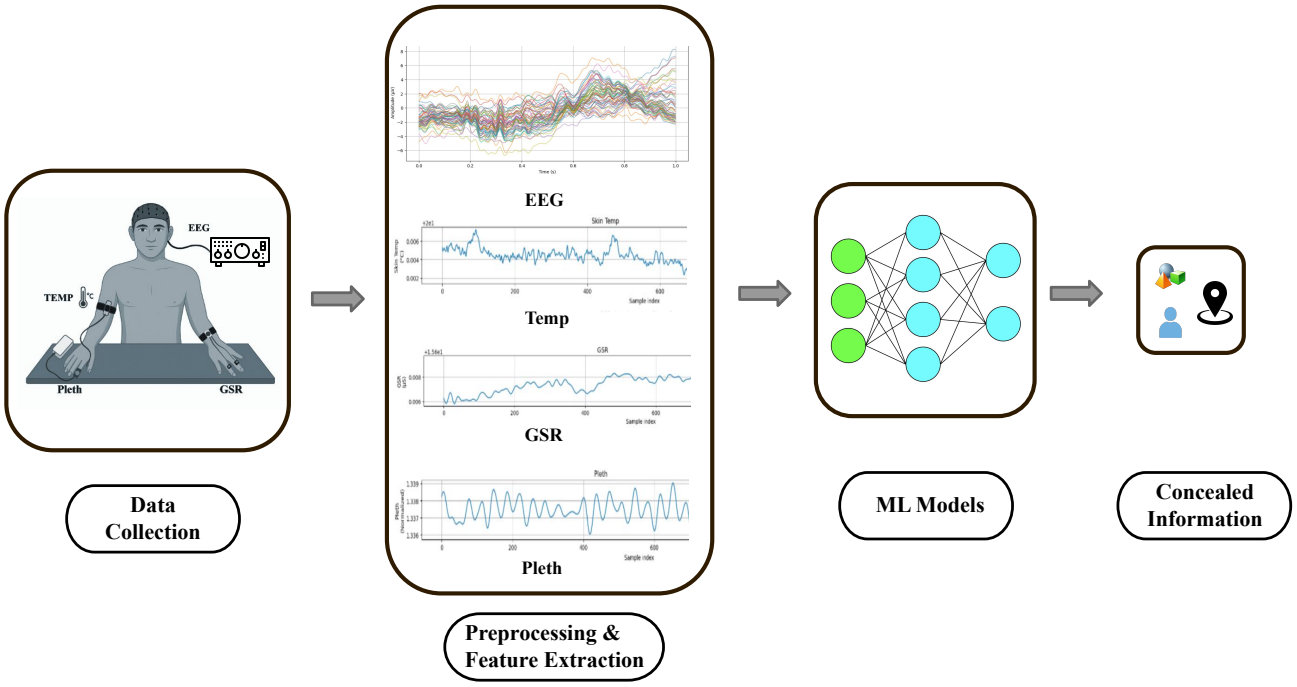

Figure 2. Analysis pipeline for multimodal concealed information detection. The workflow comprises four major stages: data collection involving simultaneous acquisition of EEG and physiological signals during CIT; preprocessing and feature extraction including artifact removal, temporal spectral feature computation, and normalization for both modalities; machine learning model training using unimodal and multimodal fusion strategies; and classification of concealed information into object, person, and place.

Physiological Signal Recording

Figure 1A illustrates the multimodal recording framework containing EEG, skin temperature (Temp), plethysmogram (Pleth), and GSR sensors used during the CIT. During the experiment, both physiological signals and EEG signals were measured and recorded with a g.tec amplifier (g.HIamp, g.tec medical engineering GmbH, Graz Austria) at a 600 Hz sampling rate, low pass filtered at 30 Hz. The temperature was recorded by g.TEMP sensor within a range of 20°C– 45°C placed on the participant's left palm. The GSR records the electrical conductivity using the two g.GSR sensor placed on the middle and ring fingertips, capturing changes in skin conductance associated with sympathetic nervous system activity. The plethysmogram were measured using a pulse oximeter sensor (g.SpO_2 sensor) attached to the left index finger. All physiological signals were filtered using a low pass filter with a cutoff below 30 Hz and a notch filter between 58–62 Hz to suppress power line noise. These electrodes were continuously monitored throughout the experimental sessions to capture autonomic responses alongside cortical activity.

Stimulus Control and Behavioral Input

In this study, we developed a custom software framework designed to deliver synchronized multimodal and behavioral data acquisition. The system integrates a MATLAB based stimulus presentation environment with a built SIMULINK module designed to ensure time synchronization with ongoing neurophysiological recordings. Stimulus onset markers were automatically generated and logged on every trial, ensuring precise alignment between external event and neurophysiological signals. Behavioral responses were captured using a Microsoft Xbox wireless controller, which was fully integrated into the software architecture for real time input monitoring.

Figure 2 illustrates the overall analysis pipeline implemented in this study. As shown, the workflow is organized into four sequential stages. First, multimodal data including EEG and physiological signals are collected in synchrony with the CIT while behavioral responses are concurrently recorded. Next, all signals undergo preprocessing and artifact removal, followed by computation of temporal and spectral features tailored to each modality. Then these features are used to train machine learning models under both unimodal and multimodal fusion strategies. Finally, the trained models perform classification of concealed information into the categories of object, person, and place.

Data Preprocessing and Artifact Removal

EEG data preprocessing was performed using the MNE-Python library. First, the raw EEG signals were bandpass filtered between 0.1 and 30 Hz to isolate frequency bands relevant for event related potential analysis. A notch filter at 60 Hz was applied to suppress power line interference. Baseline correction was then carried out using a 100 ms pre-stimulus interval to remove DC offset and low frequency drifts. Subsequently, Independent Component Analysis (ICA) was employed to detect and remove common artifacts, including those caused by eye blinks, eye movements, and muscle activity.

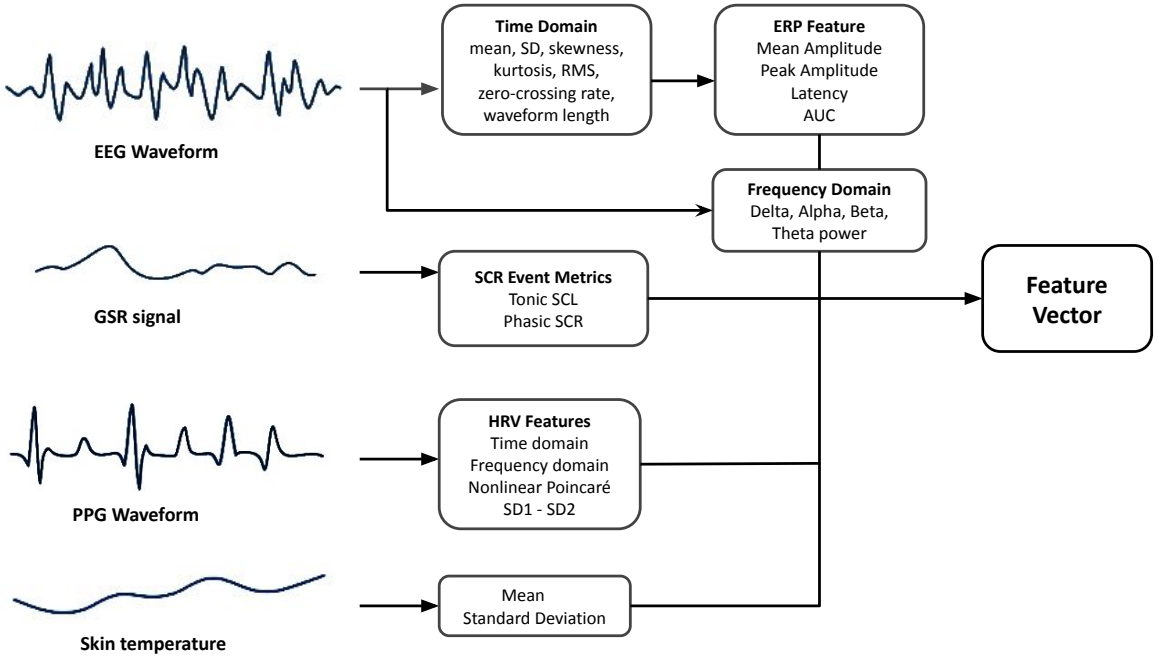

Figure 3. Feature engineering from EEG and physiological signals. The multimodal feature extraction pipeline used for concealed-information detection. EEG features comprise temporal, spectral, and ERP measures, while physiological features are derived from plethysmography, skin conductance, and temperature signals. All extracted features are concatenated into a unified multimodal feature vector for downstream classification.

Feature Engineering from EEG and Physiological Signals

Previous research has demonstrated that integrating EEG and physiological characteristics increases classification performance compared to unimodal techniques, most likely because deception involves both brain dynamics and autonomic responses[18,21,22]. EEG based deception detection often leverages ERP components and spectral features to differentiate truthful and deceptive

responses[11,36]. Physiological signals, such as GSR and HRV, have also been widely employed to detect autonomic nervous system changes indicative of deception[5,37–40]. The multimodal combination of these features enhances classification accuracy by capturing complementary aspects of physiological responses[22,41–43]. In this study, we extracted a comprehensive set of features from both EEG signals and physiological signals, including GSR, plethysmography, and skin temperature, to capture physiological markers associated with cognitive and emotional states relevant to deception detection.

Feature Extraction

EEG Feature Extraction EEG provides a direct measure of cortical activity and allows the detection of rapid neural signatures related to stimulus recognition and attention. In the context of the CIT, the P300 event-related potential is a well-established marker of concealed knowledge. It reflects attentional engagement and context updating in response to meaningful probe stimuli[7,19]. In addition to the P300, time-domain features such as mean, standard deviation, skewness, kurtosis, RMS, zero-crossing rate, and waveform length quantify signal variability and waveform characteristics. These features are linked to cognitive load and arousal[20]. Frequency-domain features, including power in delta (0.5–4 Hz), theta (4–8 Hz), alpha (8–13 Hz), and beta (13–30 Hz), capture oscillatory activity related to attention, memory, and inhibitory control, which are relevant to concealment processes[42,44]. ERP metrics such as peak amplitude, latency, mean amplitude, and area under the curve measure the magnitude and timing of neural responses to probe versus irrelevant stimuli[8,11,18,19]. EEG data were segmented into stimulus locked epochs (0.5–1.5 s) to capture event related activity. Using overlapping sliding windows of 100 milliseconds with 50 millisecond overlap ensures temporal precision and accounts for trial-to-trial variability. Together, these EEG features provide a detailed representation of the neural processes involved in recognition, attention, and intentional concealment.

Physiological Feature Extraction Autonomic physiological measures reflect the emotional and arousal components of deception, which often accompany the cognitive recognition of concealed information[13,24]. In this study, we extracted features from three peripheral signals: GSR, plethysmography, and skin temperature. GSR captures sympathetic arousal in response to probe items. The GSR time series was decomposed into tonic components, representing slower baseline skin conductance level (SCL) associated with general autonomic arousal, and phasic components, representing rapid skin conductance responses (SCR) triggered by stimuli[15,17]. Phasic responses have been shown to reliably distinguish knowledgeable from unknowledgeable subjects in CIT paradigms[31]. Features extracted from GSR included mean and standard deviation of SCL, as well as SCR metrics such as event count, amplitude, latency, and inter-response intervals, with SCR peaks above 0.1 μs considered effective responses. Plethysmography provides volumetric changes in peripheral blood flow from which heart rate and inter-beat intervals can be derived, enabling computation of pulse rate variability (PRV), a reliable surrogate for heart rate variability (HRV). Time-domain PRV features included mean of NN intervals (meanNN), standard deviation of NN intervals (SDNN), root mean square of successive NN differences (RMSNN), and the proportion of successive intervals differing by more than 50 ms (pNN50). Frequency-domain features were extracted to quantify power in low frequency (LF, 0.04–0.15 Hz) and high frequency (HF, 0.15–0.4 Hz) bands, as well as ratios such as LF/HF reflecting sympathetic-parasympathetic balance. Nonlinear Poincaré parameters SD1 and SD2 captured short- and long-term variability, respectively, providing geometric insights into autonomic regulation[22,24,25]. Skin temperature captures slower vasomotor changes linked to sympathetic activity. Statistical descriptors such as mean and standard deviation provide indices of sustained arousal and orienting responses[27,29]. Together, these features capture both rapid, transient autonomic reactions (SCR, RMSNN, SD1) and slower, sustained arousal (SCL, SD2, ST), offering a comprehensive profile of physiological responses relevant to deception detection in the CIT paradigm. All extracted features are concatenated into a unified multimodal vector for downstream classification as shown in Figure 3.

Multimodal Feature Extraction and Its Importance

Combining EEG and physiological features leverages complementary information from central and autonomic nervous system activity, providing a richer and more robust representation of the psychophysiological state. While EEG captures direct neural correlates of cognitive processes and deception related brain dynamics, physiological signals reflect autonomic responses such as emotional arousal and stress[45]. Multimodal fusion enhances the sensitivity and specificity of lie detection models by integrating these diverse physiological domains, reducing the likelihood of false positives or negatives inherent in single modality approaches[21,22,41] and has been demonstrated to improve classification performance in prior research[3,40].

Machine Learning Models

We employed multiple supervised machine learning algorithms to classify the category of concealed information (*object, person, place*) using features extracted from EEG, physiological signals , and their multimodal fusion. Algorithm selection and hyperparameter optimization were tailored to the characteristics of each modality. We evaluated logistic regression[46], support vector machine with RBF kernel[47], random forest[48], gradient boosting[49], extreme gradient boosting (XGBoost)[50], LightGBM[51], and CatBoost[52]. These models capture both linear and nonlinear dependencies, ensemble interactions, and categorical feature effects.Distinct strategies were applied to account for modality specific properties. Physiological features, which were low dimensional and relatively noise free, were modeled using logistic regression, support vector machine, random

forest, gradient boosting, and XGBoost with minimal hyperparameter tuning; features were scaled with z-score normalization and reduced via SelectKBest. EEG features were high dimensional and temporally complex; Gradient Boosting and XGBoost were optimized via grid search and validated with stratified five fold cross validation. Multimodal fusion combined EEG and physiological features, capturing cross modal interactions; ensemble boosting models (gradient boosting, XGBoost, LightGBM, CatBoost) were used with extensive hyperparameter optimization and feature ranking to maximize classification performance and interpretability.

Model Training and Evaluation All models were trained using a standardized pipeline. Categorical labels were first encoded numerically, and the top-performing features were selected using univariate statistical tests (SelectKBest). The dataset was split into stratified training (70%) and test (30%) sets, and features were standardized using z-score normalization. Models were trained on the training set with optimized hyperparameters, and performance was evaluated on the test set using accuracy, precision, recall, F1-score, Cohen's kappa, and confusion matrices. To assess generalization and robustness, five-fold stratified cross-validation was applied across EEG, physiological, and multimodal datasets.

Algorithm 1 Electrode Selection Strategy

Require: Feature matrix X (samples $\times$ features), labels y, number of electrodes $K = 8$
Ensure: Selected electrode indices S

```
Extract time-domain, frequency-domain, and ERP features for all electrodes
Train XGBoost on all features
Compute feature importance scores for each feature
Average importance scores per electrode to obtain ranked electrode list
Initialize selected set S ← ∅
while |S| < K do
    for each electrode e not in S do
        Train classifier on S ∪ {e} and compute CV accuracy
    end for
    Add electrode with highest CV accuracy to S
end while
return S
```

Electrode Selection Strategy To identify the most informative EEG electrodes, we applied a hybrid filter-wrapper approach combining XGBoost based feature importance with greedy forward selection. First, time domain, frequency domain, and ERP derived features were extracted from high density EEG for each electrode. Next, an XGBoost classifier was trained on all features to compute feature importance scores, which were averaged per electrode to obtain an initial ranking (filter step). To refine this ranking, we applied greedy forward selection: starting from the top-ranked electrode, we iteratively added electrodes that maximized five fold cross-validation accuracy of the classifier until the optimal subset of eight electrodes was selected (see Algorithm 1). This hybrid method balances interpretability (via the ranking) with predictive performance (via cross-validation) while being computationally efficient[53–56]. The resulting optimal electrode configuration (*Fp1, F7, F5, Fz, FT7, FC2, FC4, FC6*) was used for all subsequent analyses and compared with high-density EEG and the electrode layout of the iCognative device.

Results and Analysis

This study aimed to classify concealed information categories into objects, persons, and places using a multimodal approach that integrates neurophysiological signals recorded during a CIT. Multiple machine learning classifiers were evaluated, including logistic regression, support vector machine, random forest, XGBoost, gradient boosting, LightGBM, and CatBoost. Feature selection and hyperparameter tuning were applied to optimize performance.

Modality	**ML Models**				
	Logistic Regression	**Support Vector Machine**	**Random Forest**	**XGBoost**	**Gradient Boosting**
Multimodal	71.48 ± 10.19	79.98 ± 8.41	83.66 ± 7.72	90.08 ± 6.98	94.24 ± 5.74
EEG	58.07 ± 5.97	58.15 ± 7.27	70.34 ± 5.35	72.67 ± 5.93	72.98 ± 5.76
Physiological	42.30 ± 13.70	35.40 ± 4.05	54.10 ± 10.50	54.20 ± 11.25	53.40 ± 10.99

Table 1. Cross-validated classification accuracies (mean ± SD) across classifiers and modalities.

Multimodal versus Unimodal Classification Performance

Table 1 summarizes the cross-validated accuracies (mean ± SD) obtained for multimodal, unimodal EEG, and unimodal physiological features across different classifiers. Multimodal integration consistently outperformed unimodal approaches for all models. The **Gradient Boosting** classifier achieved the highest mean accuracy of **94.24 ± 5.74%**, followed by XGBoost (90.08 ± 6.98%) and CatBoost (89.72 ± 7.92%). LightGBM also demonstrated high performance (92.22 ± 6.51%). In comparison, the EEG only models achieved a maximum accuracy of 72.98 ± 5.76%, while the physiological only models reached 54.20 ± 11.25% at best, underscoring the substantial enhancement afforded by multimodal fusion. These findings confirm that the neurophysiological features provides complementary information that strengthens the decoding of concealed information categories.

Subject	CV Accuracy (%)	CV Precision (%)	CV Recall (%)	CV F1 Score (%)	Kappa (%)
Subject 1	97.4 ± 1.5	97.5 ± 1.5	97.4 ± 1.5	97.4 ± 1.5	95.8 ± 2.4
Subject 2	99.8 ± 0.4	99.8 ± 0.4	99.8 ± 0.4	99.8 ± 0.4	99.7 ± 0.6
Subject 3	99.6 ± 0.8	99.6 ± 0.8	99.6 ± 0.8	99.6 ± 0.8	99.4 ± 1.3
Subject 4	94.4 ± 3.1	94.9 ± 2.7	94.4 ± 3.1	94.2 ± 3.4	90.8 ± 5.2
Subject 5	80.2 ± 3.8	80.5 ± 3.6	80.2 ± 3.8	80.2 ± 3.8	68.1 ± 6.2
Subject 6	97.0 ± 2.0	97.1 ± 1.9	97.0 ± 2.0	97.0 ± 2.0	95.2 ± 3.3
Subject 7	87.6 ± 4.8	88.4 ± 4.4	87.6 ± 4.8	87.3 ± 5.4	79.7 ± 8.2
Subject 8	97.4 ± 1.6	97.5 ± 1.5	97.4 ± 1.6	97.4 ± 1.7	95.8 ± 2.6
Subject 9	93.8 ± 2.4	94.0 ± 2.5	93.8 ± 2.4	93.8 ± 2.4	90.0 ± 3.9
Subject 10	95.2 ± 2.8	95.4 ± 2.7	95.2 ± 2.8	95.2 ± 2.8	92.3 ± 4.5

Table 2. Cross-validation(CV) multimodal performance metrics for each subject for gradient boost model.

Statistical Comparison Among Modalities

To statistically evaluate differences in classification performance among the three modalities, a one-way repeated measures ANOVA was conducted on classification accuracies across participants. The analysis revealed a significant main effect of modality on classification accuracy, $F(2,18) = 71.40$, $p < 0.001$, $\eta_G^2 = 0.82$, indicating a large effect size. Post-hoc Bonferroni-corrected pairwise t-tests indicated that the multimodal condition (EEG + physiological signals) yielded significantly higher accuracies than both the unimodal EEG ($t(9) = -9.98$, $p < 0.001$) and physiological conditions ($t(9) = 11.38$, $p < 0.001$). Additionally, EEG performance was significantly higher than physiological ($t(9) = 4.66$, $p = 0.0035$). These results shown in Figure 4 provide strong evidence that combining EEG and physiological signals produces a robust and synergistic improvement in classification accuracy beyond either modality alone.

Subject Level Multimodal Performance

Subject wise evaluation of the gradient boosting model revealed consistently high performance across subjects as shown in Figure 5 . Individual accuracies ranged from 80.2% to 99.8%, with a group mean of 94.2 ± 5.7%. Precision, recall, and F1-scores were closely aligned (all $\approx$ 94.2 - 94.5%), indicating balanced classification performance across the three concealed information categories as well as highlighting inter-subject differences in model performance. Cohen's Kappa coefficients ranged from 68.1 ± 6.2 to 99.7 ± 0.6, with a mean of 90.7 ± 9.3, indicating substantial to almost perfect agreement beyond chance as shown in Table 2 . Notably, several subjects exhibited near perfect classification ($\geq$ 99% accuracy), demonstrating strong inter-subject generalizability and model robustness.

Overall, accurate decoding of hidden information categories was made possible by multimodal integration of neurophysiological signals, with an average accuracy of 94.2%, greatly above baselines for unimodal EEG(73%) and physiological (54.2%).

Discussion

This study introduced a multimodal framework integrating EEG and physiological signals to classify concealed information categories into objects, persons, and places recorded during CIT. Consistent with our hypotheses, the multimodal models substantially outperformed unimodal EEG and physiological approaches, demonstrating the benefits of combining neurophysiological data. The best performing Gradient Boosting model achieved a mean accuracy of 94.2%, establishing a strong benchmark for category level decoding of concealed knowledge.

Figure 6 shows the brain activity of subject 3 during the pre-stimulus, stimulus, and post-stimulus periods across different stimulus types: Object, Person and Place. Each row corresponds to different stimulus categories, with column containing

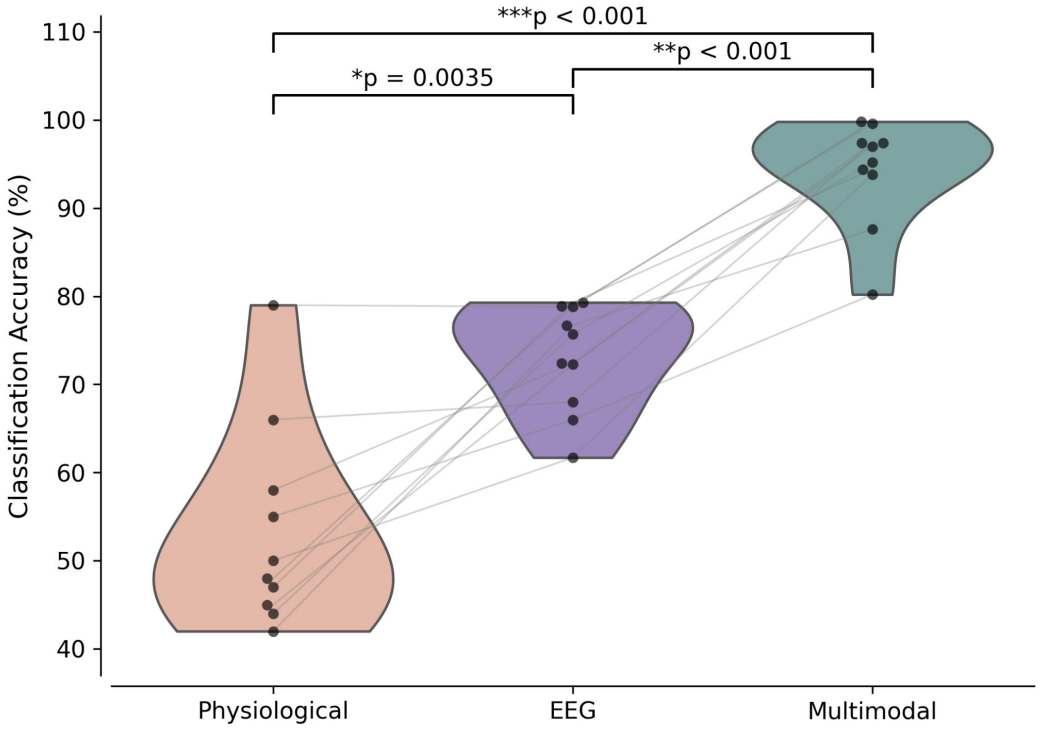

Figure 4. Statistical comparison of classification accuracy across modalities. Violin plots show the distribution of subject-level classification accuracies for physiological signals , EEG, and multimodal decoding. Each black dot represents an individual participant, and gray lines connect within-subject measurements. The repeated measures ANOVA revealed a significant main effect of modality on accuracy ($F(2,18) = 71.40$, $p < 0.001$). Post-hoc Bonferroni-corrected comparisons show that the multimodal model significantly outperforms both unimodal approaches ($p < 0.001$), and EEG also outperforms physiological signals ($p = 0.0035$).

different time points (T = -0.5s, 0.0s, 0.5s, 1.0s, 1.3s) which indicates the progression from pre-stimulus, through the stimulus presentation, to post-stimulus responses.Object related stimuli exhibit stronger posterior and occipital activation, consistent with the engagement of ventral visual object processing regions, including the lateral occipital complex[57]. Person related stimuli elicit relatively greater central and frontal activation, aligning with engagement of face selective and social processing networks, particularly the fusiform face area and adjacent frontal regions[58]. Place related stimuli display broader parietal and posterior activation, in line with spatial and scene processing networks such as the parahippocampal place area and retrosplenial cortex[59]. The temporal evolution from pre- to post-stimulus intervals reflects dynamic shifts in neural activity from anticipatory attention to active perceptual and semantic processing. These category selective topographies are consistent with theoretical neuroscience[57–59] emphasizing content specific cortical representations during concealed information paradigms.

Figure 7 presents scalp topographic activation patterns across ten subjects as they transition from a baseline state to three distinct stimulus conditions. At baseline, neural activity appears relatively uniform across subjects, providing a neutral state. In the object condition, several subjects display stronger posterior activity, consistent with activation of ventral temporal object sensitive networks that encode perceptual and semantic object knowledge[60]. In the person and place conditions, activation becomes more extensive and spatially distinct, engaging facial and scene selective networks in the ventral temporal and medial parietal cortices. From the CIT perspective, the presentation of person or place related probes may evoke not only perceptual but also memory based orienting or inhibition signals, because these stimuli could carry concealed significance to the participant. CIT research has shown that memory relevant probes (versus irrelevants) elicit enhanced neural or autonomic responses such as larger P300 amplitudes or differential frontal negative slow waves interpreted under the orienting response or arousal inhibition frameworks[61]. Thus, the gradation from baseline to object to person/place may reflect increasing stimulus salience or meaningfulness to the subject, and accordingly, the brain maps show more robust activation (red) when the stimulus type likely overlaps with the concealed information category.

We further investigated the impact of reducing electrode based electrode selection strategy described above on classification performance. Three electrode configurations were compared: (i) the full 64-electrode montage (High Density Configuration),

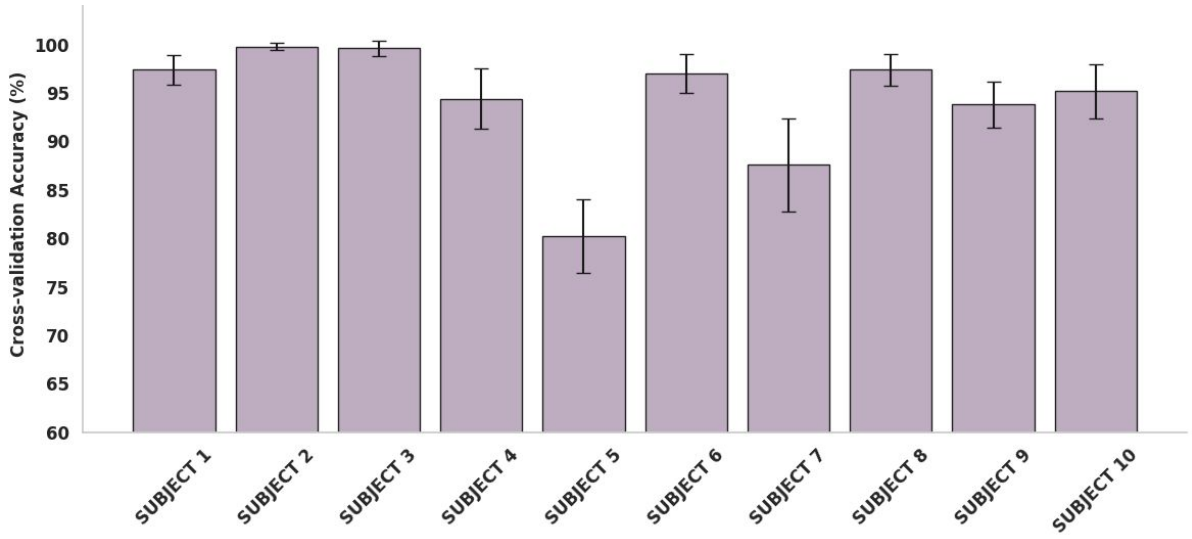

Figure 5. Per-subject classification accuracy using gradient boost model on mutimodal data. Bar plots show cross-validated accuracy for each participant, with error bars representing standard deviation across folds. Accuracy varies across individuals, highlighting inter-subject differences in model performance.

(ii) an optimized subset of eight electrodes derived from a hybrid feature importance and forward selection procedure (Optimal Configuration), and (iii) the same eight-electrode configuration employed in BrainWave Science's wearable device (iCognative Configuration). From Table 3, it is evident that the multimodal condition for both reduced configurations maintained high accuracy, exceeding the performance of the full 64-electrode system. The Optimal Configuration achieved $99.18 \pm 0.68\%$ accuracy, performing nearly identically to the iCognative Configuration ($99.02 \pm 1.55\%$) for the Gradient Boosting model, and slightly surpassing the high-density configuration ($94.24 \pm 5.74\%$). Similarly from Table 4, in the unimodal EEG condition, the Optimal configuration ($68.69 \pm 3.48\%$) and the iCognative configuration ($65.74 \pm 5.49\%$) performed comparably to the high-density configuration ($72.98 \pm 5.76\%$). These findings demonstrate that robust multimodal classification can be achieved using a low-density EEG system when electrodes are strategically selected.

To better understand the contribution of different signals, we performed feature importance analysis across physiological and EEG features. Among physiological features, mean skin conductance level (*mean_scl*), SD2, SDNN, RMSNN, and SD1 were highly informative, reflecting autonomic arousal and stress responses linked to cognitive load during deception, with *mean_scl* emerging as a particularly robust indicator. Heart rate variability features such as SDNN and RMSNN also

ML Models	**Different Electrode Configuration**		
	iCognative Configuration	**Optimal Configuration**	**High Density Configuration**
Logistic Regression	63.00 ± 12.56	63.82 ± 11.08	71.48 ± 10.19
Support Vector Machine	49.34 ± 5.84	49.58 ± 4.87	79.98 ± 8.41
Random Forest	89.52 ± 5.52	89.72 ± 6.07	83.66 ± 7.72
XGBoost	97.64 ± 2.87	97.88 ± 1.61	90.08 ± 6.98
Gradient Boosting	99.02 ± 1.55	99.18 ± 0.68	94.24 ± 5.74
LightGBM	98.58 ± 2.30	98.90 ± 0.92	92.22 ± 6.51
CatBoost	97.06 ± 3.56	97.00 ± 2.22	89.72 ± 7.92

Table 3. Multimodal classification accuracy (%) aross different machine learning models and electrode configurations.

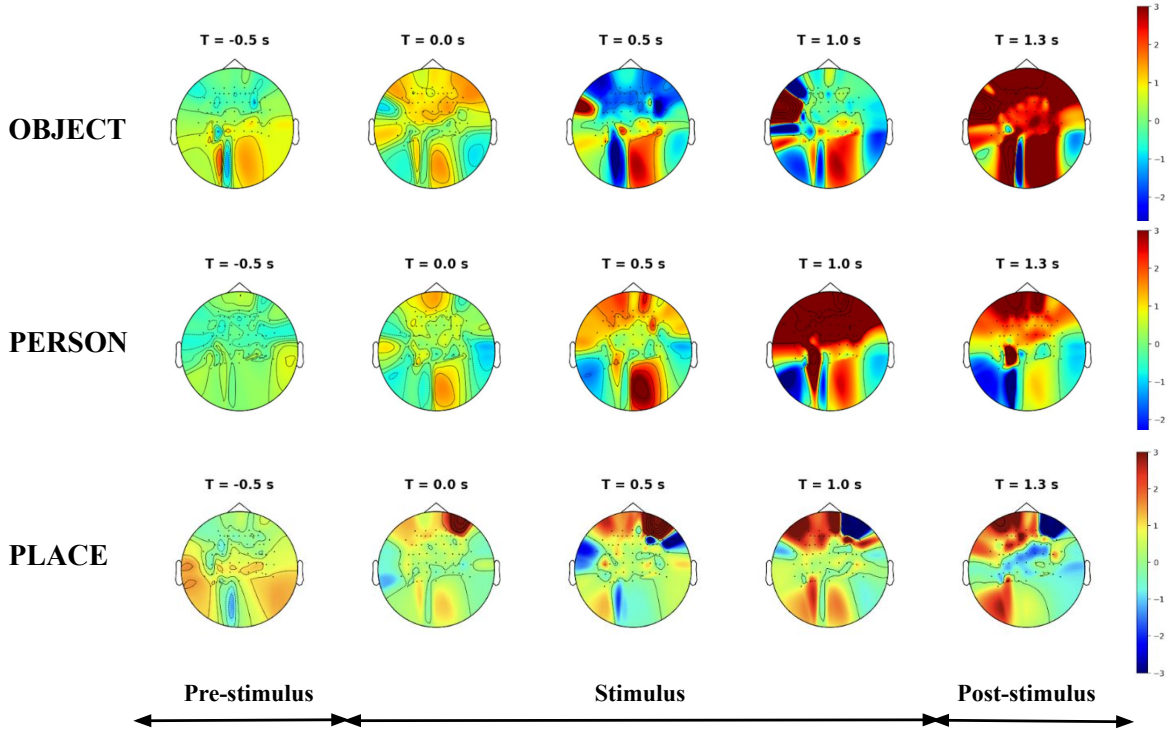

Figure 6. Subject 3 scalp topography plots. Scalp topographic plots of subject 3 across differnt time pointsmaps showing the brain activity during the pre-stimulus, stimulus, and post-stimulus periods across different stimulus types (Object, Person, Place). Each row corresponds to different stimulus categories, with time points (T = -0.5s, 0.0s, 0.5s, 1.0s, 1.3s) displayed in the columns indicates the progression from pre-stimulus, through the stimulus presentation, to post-stimulus responses. The color bar represents z-score normalization of the EEG signal within a 300 ms window, with red representing high activity and blue indicating low activity.

contributed significantly, consistent with prior studies showing that autonomic cardiac responses are sensitive to stress and cognitive effort. EEG features exhibiting the highest importance included root mean square amplitude, ERP latency, alpha band power, and peak amplitude at electrode C1, capturing both temporal and spatial neural dynamics associated with attentional and cognitive processes during deception. Additional features, including zero crossing rate at AF8 and waveform length at Cz, reflected finer aspects of signal complexity beyond simple amplitude measures. While features at C1 were highly ranked, the electrode selection procedure prioritized a subset that maximized classification accuracy while reducing redundancy across features. As a result, the final optimal electrode set (Fp1, F7, F5, Fz, FT7, FC2, FC4, FC6) spans prefrontal and frontocentral regions, collectively capturing complementary neural and physiological information such as ERP timing, alpha power, and autonomic responses. This explains why C1, despite its high feature-level importance, was not included in the reduced montage, as its contribution overlapped with other selected electrodes. Integration of physiological and EEG signals in the multimodal framework further enhanced classification performance, with autonomic markers remaining highly informative and EEG-derived features at the selected prefrontal and frontocentral electrodes providing complementary information. In

ML Models	**Different Electrode Configuration**		
	iCognative Configuration	**Optimal Configuration**	**High Density Configuration**
Logistic Regression	52.67 ± 5.12	52.86 ± 4.34	58.07 ± 5.97
Support Vector Machine	50.81 ± 7.87	52.83 ± 5.28	58.15 ± 7.27
Random Forest	64.71 ± 5.35	66.30 ± 3.32	70.34 ± 5.35
XGBoost	65.68 ± 5.25	68.26 ± 4.47	72.67 ± 5.93
Gradient Boosting	65.74 ± 5.49	68.69 ± 3.48	72.98 ± 5.76

Table 4. Unimodal EEG classification accuracy (%) across different machine learning models and electrode configurations.

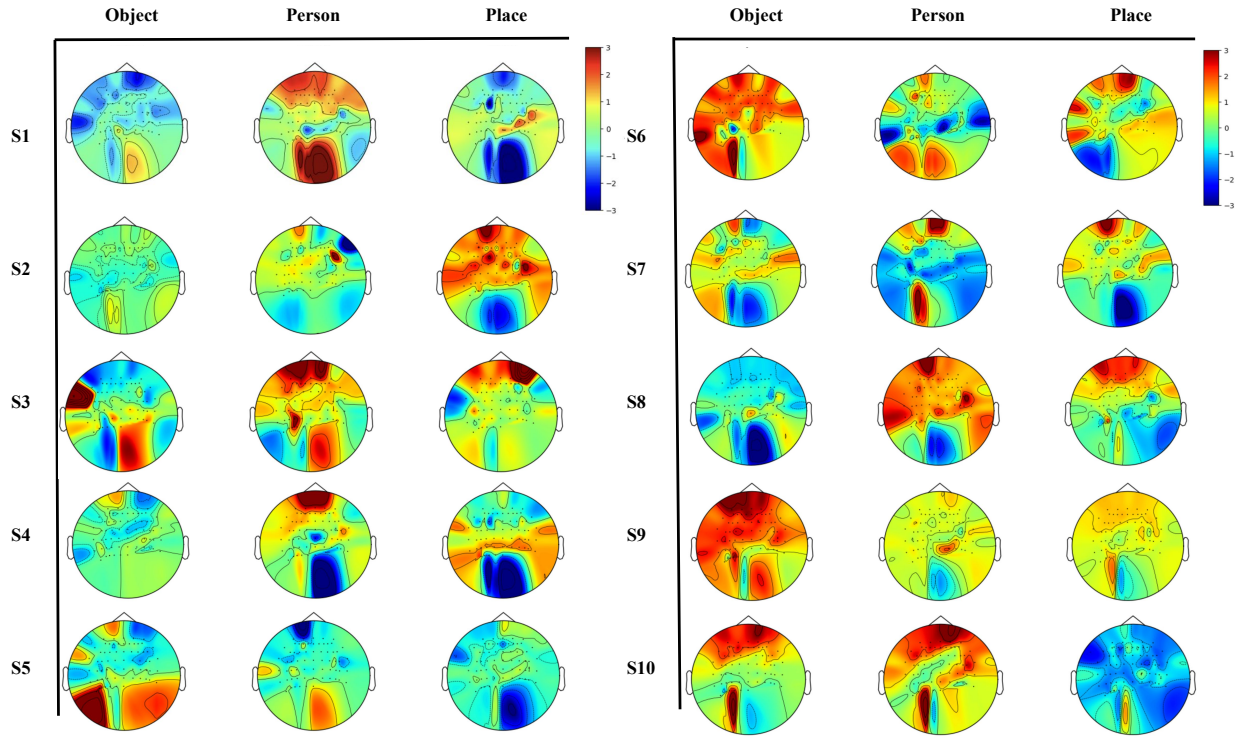

Figure 7. EEG topographic maps for all participants across stimuli. The topographic maps displays the brain activity dynamics for 10 participants (S1 to S10) across object, person, and place stimuli. The color bar represents z-score normalization of the EEG signal within a 300 ms window. The figure highlights individual variability in neural responses across different stimuli.

particular, ERP latency at *FC6* underscores the relevance of timing information from frontal-central regions in detecting deceptive responses. The eight-electrode configuration effectively covers regions implicated in executive control, conflict monitoring, and affective regulation, processes known to be engaged during deception and associated with sympathetic arousal and cognitive inhibition. Frontal midline theta oscillations and slow-wave activity captured by these electrodes are sensitive to mental effort and emotional tension, demonstrating that the selected set balances coverage of both neural and autonomic processes while minimizing redundancy. While the iCognative® platform demonstrates practical applicability of EEG-based concealed information detection, our results indicate that high decoding accuracy can be achieved with a low-density EEG setup when combined with physiological sensors.

A central implication of these findings is that concealed information, as elicited by the CIT, is best understood as a distributed cognitive state rather than a singular neural event. The observed gains from multimodal integration suggest that concealment engages at least two partially dissociable processes: (i) rapid perceptual semantic access to stimulus content and its mnemonic relevance, indexed by EEG dynamics such as ERP latency and oscillatory modulation, and (ii) sustained autonomic regulation reflecting arousal, conflict, and response inhibition, indexed by skin conductance and heart rate variability. Importantly, neither process alone was sufficient to achieve high decoding accuracy across subjects. This interpretation is consistent with theoretical models of the CIT proposing that detection effects arise from the interaction between orienting responses to meaningful stimuli and top–down control mechanisms that regulate overt responding under concealment demands[8]. From this perspective, EEG features primarily capture the timing and allocation of attentional and executive resources associated with stimulus evaluation and response control[62], whereas physiological measures reflect the downstream consequences of these processes on autonomic state, including sympathetic arousal and cardiac regulation[63]. The success of ensemble-based multimodal models further suggests that these components interact in a nonlinear manner, consistent with the notion that concealed knowledge is not expressed uniformly across individuals or trials but fluctuates as a function of cognitive load, emotional salience, and control efficacy[24].

This interpretation also helps explain why reduced, fronto-central electrode montages were sufficient for high performance in the multimodal condition. Rather than requiring fine grained spatial resolution across the entire cortex, effective decoding appears to depend on capturing control related neural dynamics that integrate perceptual input with autonomic regulation.

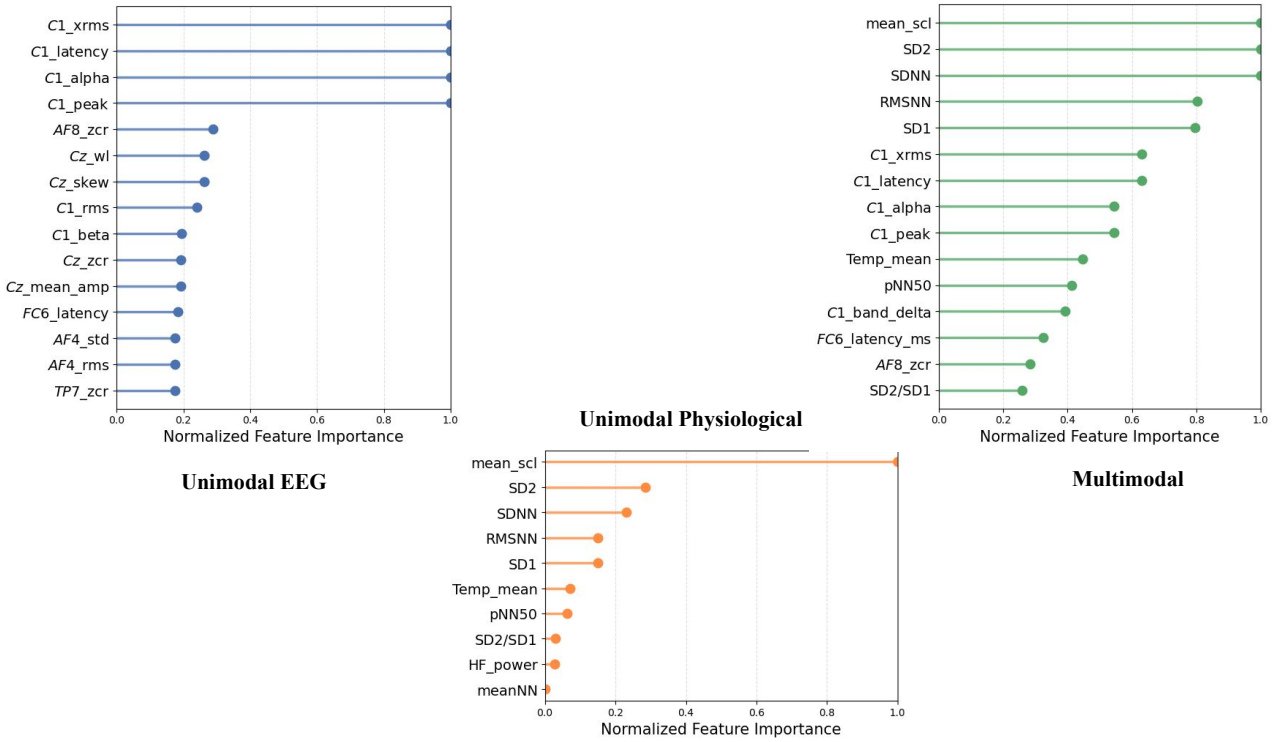

Figure 8. Feature importance across unimodal and multimodal conditions. Feature importance scores obtained using the SelectKBest method for three feature sets: unimodal physiological features (orange), unimodal EEG features (blue), and multimodal features combining EEG and physiological signals (green). The Feature importance scores are normalized for better visualisation.

Fronto-central regions are well positioned to mediate this integration, given their established role in conflict monitoring, inhibitory control, and regulation of physiological arousal. The absence of performance gains from high density EEG suggests that additional electrodes may introduce redundancy or noise without substantially increasing access to the cognitive variables most relevant to concealment. This challenges the assumption that maximal electrode coverage is inherently advantageous for applied neurophysiological classification and instead emphasizes the importance of task-informed electrode selection.

At the same time, the present results delineate important boundary conditions. The high accuracies reported here were obtained under controlled experimental conditions with predefined stimulus categories and limited variability in task structure. Concealed information in applied contexts may involve more complex, overlapping, or emotionally salient representations, which could alter the balance between neural and autonomic contributions[8]. Moreover, the current framework does not explicitly model strategic countermeasures or individual differences in cognitive control capacity, both of which are known to modulate CIT related neural and autonomic responses[14,24]. Addressing these factors will be essential for determining the robustness and generalizability of multimodal concealed information detection beyond laboratory settings.

Conclusion

This study introduced a multimodal framework for classifying the category of concealed information into objects, persons, and places by integrating neurophysiological signals recorded during a CIT. Through systematic comparison across machine learning models and modalities, the proposed approach demonstrated a substantial improvement in decoding accuracy compared to unimodal EEG and physiological inputs. The Gradient Boosting model achieved the highest overall performance, yielding a mean classification accuracy of 94.24% across subjects, significantly surpassing unimodal EEG (72.98%) and unimodal physiological (53.4%) baselines. Statistical analysis confirmed that multimodal fusion provides a robust and complementary advantage,which signifies the importance of combining neurophysiological measures in detecting concealed knowledge. Another key contribution of this work lies in the electrode selection strategy, which identified a compact subset of eight electrodes primarily distributed across prefrontal and frontocentral regions as sufficient for maintaining high decoding accuracy. These regions are well known for their involvement in executive control and stress related cognitive load, consistent with established neurophysiological correlates of deception. Furthermore, benchmarking with electrode configuration of iCognative® device

demonstrated that comparable performance can be achieved with low density, research grade EEG configuration. This finding underscores the potential for future translation of the proposed approach into practical, portable, and scalable applications. In summary, the present work demonstrates that accurate decoding of concealed information categories can be achieved using a compact multimodal configuration. By uniting data driven electrode selection with cognitive neuroscientific principles, this study bridges laboratory grade EEG research with emerging wearable neurotechnology. By bridging cognitive neuroscience and computational modeling, this study advances the feasibility of interpretable, neurophysiology based forensic technologies. Future work will focus on expanding the dataset to diverse populations, incorporating real time signal processing, and exploring deep learning architectures for end-to-end multimodal fusion, thereby moving closer to deployment of neurophysiological deception detection in applied settings.

Data availability

The dataset of this study are available from the corresponding author on reasonable request.

Ethics statement

The studies involving humans were approved by the present study was conducted under IRB Approved Protocol at the University of Maryland Baltimore County (Protocol #408 – Selection of Optimal Control Signals for Human Machine Interfaces). The studies were conducted in accordance with the local legislation and institutional requirements. The participants provided their written informed consent to participate in this study.

References

1. Rosenfeld, J. P. (ed.) *Detecting Concealed Information and Deception: Recent Developments* (Elsevier / Academic Press, London / New York, 2018). DOI: 10.1016/B978-0-12-812729-2.00001-X.
2. Honts, C. R. The psychophysiological detection of deception. *The detection deception forensic contexts* 103–123, DOI: 10.1017/CBO9780511490071.005 (2004).
3. Podlesny, J. A. & Raskin, D. C. Physiological measures and the detection of deception. *Psychol. bulletin* **84**, 782, DOI: 10.1037/0033-2909.84.4.782 (1977).
4. Ben-Shakhar, G. & Furedy, J. J. *Theories and applications in the detection of deception: A psychophysiological and international perspective* (Springer Science & Business Media, 2012). DOI: 10.1007/978-1-4612-3282-7.
5. Lykken, D. T. The gsr in the detection of guilt. *journal Appl. Psychol.* **43**, 385, DOI: 10.1037/h0046060 (1959).
6. Polich, J. & Kok, A. P300, probability, and interstimulus interval. *Psychophysiology* **27**, 396–403, DOI: 10.1111/j.1469-8986.1990.tb02333.x (1990).
7. Rosenfeld, J. P., Soskins, M., Bosh, G. & Ryan, A. Simple, effective countermeasures to p300-based tests of detection of concealed information. *Psychophysiology* **41**, 205–219, DOI: 10.1111/j.1469-8986.2004.00158.x (2004).
8. Verschuere, B., Ben-Shakhar, G. & Meijer, E. *Memory detection: Theory and application of the Concealed Information Test* (Cambridge University Press, 2011). DOI: 10.1017/CBO9780511975196.
9. Rosenfeld, J. P. P300 in detecting concealed information and deception: A review. *Psychophysiology* **57**, e13362, DOI: 10.1111/psyp.13362 (2020).
10. Simbolon, A. I., Turnip, A., Hutahaean, J., Siagian, Y. & Irawati, N. An experiment of lie detection based eeg-p300 classified by svm algorithm. In *2015 International Conference on Automation, Cognitive Science, Optics, Micro Electro-Mechanical System, and Information Technology (ICACOMIT)*, 68–71, DOI: 10.1109/ICACOMIT.2015.7440177 (IEEE, 2015).
11. Abootalebi, V., Moradi, M. H. & Khalilzadeh, M. A. A new approach for eeg feature extraction in p300-based lie detection. *Comput. methods programs biomedicine* **94**, 48–57, DOI: 10.1016/j.cmpb.2008.10.001 (2009).
12. Wang, H., Chang, W. & Zhang, C. Functional brain network and multichannel analysis for the p300-based brain computer interface system of lying detection. *Expert. Syst. with Appl.* **53**, 117–128, DOI: 10.1016/j.eswa.2016.01.024 (2016).
13. Ben-Shakhar, G. & Elaad, E. The validity of psychophysiological detection of information with the guilty knowledge test: A meta-analytic review. *J. Appl. Psychol.* **88**, 131, DOI: 10.1037/0021-9010.88.1.131 (2003).
14. Rosenfeld, J. P., Soskins, M., Bosh, G. & Ryan, A. Simple, effective countermeasures to p300-based tests of detection of concealed information. *Psychophysiology* **41**, 205–219, DOI: 10.1111/j.1469-8986.2004.00158.x (2004).

15. Ben-Shakhar, G. A further study of the dichotomization theory in detection of information. *Psychophysiology* **14**, 408–413, DOI: 10.1111/j.1469-8986.1977.tb02974.x (1977).

16. Cutrow, R. J., Parks, A., Lucas, N. & Thomas, K. The objective use of multiple physiological indices in the detection of deception. *Psychophysiology* **9**, 578–588, DOI: 10.1111/j.1469-8986.1972.tb00767.x (1972).

17. Lykken, D. T. The validity of the guilty knowledge technique: The effects of faking. *J. Appl. Psychol.* **44**, 258, DOI: 10.1037/h0044413 (1960).

18. Rosenfeld, J. P. Event-related potentials in the detection of deception, malingering, and false memories. (2002).

19. Meixner, J. B. & Rosenfeld, J. P. A mock terrorism application of the p300-based concealed information test. *Psychophysiology* **48**, 149–154, DOI: 10.1111/j.1469-8986.2010.01050.x (2011).

20. Bablani, A., Edla, D. R. & Dodia, S. Classification of eeg data using k-nearest neighbor approach for concealed information test. *Procedia computer science* **143**, 242–249, DOI: 10.1016/j.procs.2018.10.392 (2018).

21. Ambach, W., Bursch, S., Stark, R. & Vaitl, D. A concealed information test with multimodal measurement. *Int. J. Psychophysiol.* **75**, 258–267, DOI: 10.1016/j.ijpsycho.2009.12.007 (2010).

22. Farahani, E. D. & Moradi, M. H. Multimodal detection of concealed information using genetic-svm classifier with strict validation structure. *Informatics Medicine Unlocked* **9**, 58–67, DOI: 10.1016/j.imu.2017.05.004 (2017).

23. Farahani, E. & Moradi, M. A concealed information test with combination of erp recording and autonomic measurements. *Neurophysiology* **45**, 223–233, DOI: 10.1016/j.ijpsycho.2009.12.007 (2013).

24. Gamer, M. Detecting concealed information using autonomic measures. *Mem. detection: Theory application Concealed Inf. Test* 27–45, DOI: 10.1017/CBO9780511975196.003 (2011).

25. Bradley, M. & Janisse, M. P. Accuracy demonstrations, threat, and the detection of deception: Cardiovascular, electrodermal, and pupillary measures. *Psychophysiology* **18**, 307–315, DOI: 10.1111/j.1469-8986.1981.tb03040.x (1981).

26. Ben-Shakhar, G. & Dolev, K. Psychophysiological detection through the guilty knowledge technique: effects of mental countermeasures. *J. applied psychology* **81**, 273, DOI: 10.1037/0021-9010.81.3.273 (1996).

27. Pollina, D. A. *et al.* Facial skin surface temperature changes during a "concealed information" test. *Annals biomedical Eng.* **34**, 1182–1189, DOI: 10.1007/s10439-006-9143-3 (2006).

28. Park, K. K., Suk, H. W., Hwang, H. & Lee, J.-H. A functional analysis of deception detection of a mock crime using infrared thermal imaging and the concealed information test. *Front. human neuroscience* **7**, 70, DOI: 10.3389/fnhum.2013.00070 (2013).

29. Warmelink, L. *et al.* Thermal imaging as a lie detection tool at airports. *Law human behavior* **35**, 40–48, DOI: 10.1007/s10979-010-9251-3 (2011).

30. Liu, I., Liu, F., Zhong, Q., Ma, F. & Ni, S. Your blush gives you away: detecting hidden mental states with remote photoplethysmography and thermal imaging. *PeerJ Comput. Sci.* **10**, e1912, DOI: 10.7717/peerj-cs.1912 (2024).

31. Ambach, W. & Gamer, M. Physiological measures in the detection of deception and concealed information. In *Detecting concealed information and deception*, 3–33, DOI: 10.1016/B978-0-12-812729-2.00001-X (Elsevier, 2018).

32. Koelstra, S. *et al.* Deap: A database for emotion analysis; using physiological signals. *IEEE transactions on affective computing* **3**, 18–31, DOI: 10.1109/T-AFFC.2011.15 (2011).

33. Brouwer, A.-M. *et al.* Estimating workload using eeg spectral power and erps in the n-back task. *J. neural engineering* **9**, 045008, DOI: 10.1088/1741-2560/9/4/045008 (2012).

34. Haxby, J. V. *et al.* Distributed and overlapping representations of faces and objects in ventral temporal cortex. *Science* **293**, 2425–2430, DOI: 10.1126/science.1063736 (2001).

35. Haynes, J.-D. A primer on pattern-based approaches to fmri: principles, pitfalls, and perspectives. *Neuron* **87**, 257–270, DOI: 10.1016/j.neuron.2015.05.025 (2015).

36. Farwell, L. A. Brain fingerprinting: a comprehensive tutorial review of detection of concealed information with event-related brain potentials. *Cogn. neurodynamics* **6**, 115–154, DOI: 10.1007/s11571-012-9192-2 (2012).

37. Duran, G., Tapiero, I. & Michael, G. A. Resting heart rate: A physiological predicator of lie detection ability. *Physiol. & behavior* **186**, 10–15, DOI: 10.1016/j.physbeh.2018.01.002 (2018).

38. Cook, L. G. & Mitschow, L. C. Beyond the polygraph: Deception detection and the autonomic nervous system. *Fed. Pract.* **36**, 316 (2019).

39. Block, J. A study of affective responsiveness in a lie-detection situation. *The J. Abnorm. Soc. Psychol.* **55**, 11, DOI: 10.1037/h0046624 (1957).

40. Vrij, A. *Detecting lies and deceit: Pitfalls and opportunities* (Wiley, 2008).

41. Joshi, G. *et al.* Multimodal machine learning for deception detection using behavioral and physiological data. *Sci. Reports* **15**, 8943, DOI: 10.1038/s41598-025-92399-6 (2025).

42. Taha, B. N., Baykara, M. & Alakuş, T. B. Neurophysiological approaches to lie detection: A systematic review. *Brain Sci.* **15**, 519, DOI: 10.3390/brainsci15050519 (2025).

43. Javaid, H., Dilawari, A., Khan, U. G. & Wajid, B. Eeg guided multimodal lie detection with audio-visual cues. In *2022 2nd International conference on artificial intelligence (ICAI)*, 71–78, DOI: 10.1109/ICAI55435.2022.9773469 (IEEE, 2022).

44. Saini, N., Bhardwaj, S. & Agarwal, R. Classification of eeg signals using hybrid combination of features for lie detection. *Neural Comput. Appl.* **32**, 3777–3787, DOI: 10.1007/s00521-019-04078-z (2020).

45. Kugelmass, S. & Lieblich, I. Effects of realistic stress and procedural interference in experimental lie detection. *J. Appl. Psychol.* **50**, 211, DOI: 10.1037/h0023324 (1966).

46. Hosmer Jr, D. W., Lemeshow, S. & Sturdivant, R. X. *Applied logistic regression* (John Wiley & Sons, 2013).

47. Cortes, C. & Vapnik, V. Support-vector networks. *Mach. learning* **20**, 273–297, DOI: 10.1007/BF00994018 (1995).

48. Breiman, L. Random forests. *Mach. learning* **45**, 5–32 (2001).

49. Friedman, J. H. Greedy function approximation: A gradient boosting machine. *Annals Stat.* **29**, 1189–1232, DOI: 10.1214/aos/1013203451 (2001).

50. Chen, T. & Guestrin, C. Xgboost: A scalable tree boosting system. In *Proceedings of the 22nd ACM SIGKDD International Conference on Knowledge Discovery and Data Mining*, 785–794, DOI: 10.1145/2939672.2939785 (San Francisco, CA, USA, 2016).

51. Ke, G. *et al.* Lightgbm: A highly efficient gradient boosting decision tree. vol. 30 (2017).

52. Prokhorenkova, L., Gusev, G., Vorobev, A., Dorogush, A. V. & Gulin, A. Catboost: unbiased boosting with categorical features. In *Advances in Neural Information Processing Systems (NeurIPS)*, 6638–6648 (2018).

53. Lotte, F., Congedo, M., Lécuyer, A., Lamarche, F. & Arnaldi, B. A review of classification algorithms for eeg-based brain–computer interfaces: a 10 year update. *J. Neural Eng.* **15**, 031005, DOI: 10.1088/1741-2552/aab2f2 (2018).

54. Alotaiby, T., El-Samie, F. E. A., Alshebeili, S. A. & Ahmad, I. A review of channel selection algorithms for eeg signal processing. *EURASIP J. on Adv. Signal Process.* **2015**, 66, DOI: /10.1186/s13634-015-0251-9 (2015).

55. Blankertz, B., Lemm, S., Treder, M., Haufe, S. & Müller, K.-R. Single-trial analysis and classification of erp components—a tutorial. In *NeuroImage*, vol. 56, 814–825, DOI: 10.1016/j.neuroimage.2010.06.048 (Elsevier, 2011).

56. Bashivan, P., Rish, I., Yeasin, M. & Codella, N. Learning representations from eeg with deep recurrent-convolutional neural networks. DOI: 10.48550/arXiv.1511.06448 (2015).

57. Grill-Spector, K., Kushnir, T., Edelman, S., Itzchak, Y. & Malach, R. Cue-invariant activation in object-related areas of the human occipital lobe. *Neuron* **21**, 191–202, DOI: 10.1016/S0896-6273(00)80526-7 (1998).

58. Kanwisher, N., McDermott, J. & Chun, M. M. The fusiform face area: a module in human extrastriate cortex specialized for face perception. *J. Neurosci.* **17**, 4302–4311, DOI: 10.1523/JNEUROSCI.17-11-04302.1997 (1997).

59. Epstein, R. & Higgins, J. S. Differential parahippocampal and retrosplenial involvement in three types of visual scene recognition. *Cereb. Cortex* **17**, 1680–1693, DOI: 10.1093/cercor/bhl079 (2007).

60. Martin, A. Neural substrates of object identification: Functional magnetic resonance imaging evidence that category and visual attribute contribute to semantic knowledge. *J. Int. Neuropsychol. Soc.* **6**, 320–335, DOI: 10.1017/S1355617700633054 (2000).

61. Rosenfeld, J. P., Ben-Shakhar, G. & Meijer, E. Advances in concealed information testing: Eeg and psychophysiological markers of recognition. *Behav. Sci.* **14**, 627, DOI: 10.3390/bs14080627 (2024).

62. Polich, J. Updating p300: An integrative theory of p3a and p3b. *Clin. Neurophysiol.* **118**, 2128–2148, DOI: 10.1016/j.clinph.2007.04.019 (2007).

63. Thayer, J. F., Ahs, F., Fredrikson, M., Sollers, J. J. I. & Wager, T. D. A meta-analysis of heart rate variability and neuroimaging studies: implications for heart rate variability as a marker of stress and health. *Neurosci. & Biobehav. Rev.* **36**, 747–756, DOI: 10.1016/j.neubiorev.2011.11.009 (2012).

Acknowledgements

This research was funded by the National Science Foundation (NSF) CAREER Award, grant number IIS-2053498 and NSF IUCRC Phase II UMBC: BRAIN, grant number CNS-2333292.

Author contributions

Conceptualization, S.S, R.V, K.I and S.K; methodology, S.S, R.V, K.I and S.K; experiment, S.S, R.V, K.I and S.K; formal analysis, S.S and S.K; writing-original draft preparation, S.S, and R.V; writing-review and editing, S.S and R.V. All authors have read and agreed to the published version of the manuscript.

Conflict of Interest

The authors declare that the research was conducted in the absence of any commercial or financial relationships that could be construed as a potential conflict of interest.

Corresponding Author

Correspondence and requests for materials should be addressed to Ramana Vinjamuri.